Effect of the Excitation Energy on the (HI)₂ Nonadiabatic Photodissociation Dynamics

S. López-López, R. Prosmiti, and A. García-Vela*

Instituto de Matematicas y Física Fundamental, C.S.I.C., Serrano 123, 28006 Madrid, Spain

Received: November 8, 2007; In Final Form: January 14, 2008

The effect of the excitation energy on the nonadiabatic photodissociation dynamics of (HI)₂ is explored in this work. A wave packet model is applied that simulates the photodissociation process starting from the I*–HI complex left behind after dissociation of the first HI moiety within (HI)₂. The probability and product fragment state distributions of the different photodissociation pathways are analyzed in a wide range of excitation energies of the I*–HI absorption spectrum. It is found that the probability of electronically nonadiabatic transitions increases substantially (by a factor larger than two) in the range of excitation energies analyzed. This increase is due to an enhancement of the intensity of the spin–rotation coupling responsible for the nonadiabatic transitions with increasing excitation energy. A remarkably high fraction of bound, highly excited I₂ photoproducts, slowly decreasing as the excitation energy increases, is also found over the range of energies studied. The I₂ product state distributions show manifestations of rotational interference effects and also of rotational cooling in the case of the I₂ state distributions produced upon nonadiabatic transitions. Such effects become more pronounced with increasing energy. Experimental implications of these findings are discussed.

I. Introduction

Manifestations of nonadiabatic effects are often encountered in photochemical processes occurring in small molecules and clusters.[1] Such manifestations are typically produced when the molecule or cluster contains heavy atoms that give rise to significant relativistic effects that are able to couple different electronic states of the system (e.g., through interactions like spin–orbit, spin–rotation, etc.).[2–18] Nonadiabatic transitions take place between the coupled electronic states, leaving a signature in observable quantities that provides information about the underlying nonadiabatic dynamics.

An interesting case arises when the electronically nonadiabatic transitions are mediated by intracluster collisions occurring between the nascent fragments produced upon photodissociation of a cluster system. The intracluster collisions that induce the nonadiabatic transitions are favored by the cluster geometry initially prepared before photodissociation. In this situation the nonadiabatic process and its manifestations become dependent, to a certain extent, on the conditions in which the intracluster collisions take place. Elucidating such a dependence is a central issue in order to understand in detail this type of nonadiabatic photodissociation dynamics.

An example of the above nonadiabatic process has been reported experimentally for the photodissociation of small (HI)ₙ clusters, where $n = 2$ was the dominant cluster size, with 266 nm radiation.[19] The main finding of these experiments was the observation of a small peak at very high energies in the measured translational energy spectrum of hydrogen fragments. This peak (referred to as β peak in ref 19) accounted for 0.1–1% out of the total signal of the translational energy spectrum. The position of the β peak was separated from the higher energy peak resulting from photolysis of the HI monomer by an amount of energy nearly equal to the spin–orbit splitting between the I($^2P_{3/2}$) and I($^2P_{1/2}$) electronic states (hereafter denoted as I and

I*, respectively) of the iodine fragment, namely, $\Delta = 7603$ cm⁻¹.[20] The observed β peak associated with very fast H fragments was attributed to an electronically nonadiabatic transition through spin–rotation coupling, occurring upon sequential photodissociation of the (HI)ₙ clusters.[19] In a first step, photodissociation of a HI moiety within (HI)ₙ produces an I*–(HI)ₙ₋₁ complex, and a second HI dissociation within I*–(HI)ₙ₋₁ generates a H fragment that can undergo an intracluster collision with I*, causing in some events its deactivation to the ground state I via a nonadiabatic transition. As a result of this intracluster collision, the scattered H fragment acquires as additional translational energy, nearly all the excitation energy of I* ($\Delta = 7603$ cm⁻¹), giving rise to the observed β peak at high H kinetic energies in the spectrum.

Wave packet simulations of the (HI)₂ nonadiabatic photodissociation were reported recently,[21,22] and they confirmed the mechanism proposed in ref 19 to explain the appearance of the β peak in the H fragment spectrum. The model applied in the simulations took advantage of the sequential character of the (HI)₂ photodissociation dynamics. More specifically, it was assumed in the model that photodissociation of the first HI moiety within (HI)₂ has taken place in a first step, leaving behind an I*–HI complex. Then, the second step of the sequential photodissociation dynamics, namely, the photodissociation of the remaining HI subunit within I*–HI, was simulated by means of a three-dimensional nonadiabatic wave packet treatment. Such a treatment involved photodissociation of the system on two coupled excited electronic surfaces corresponding to the I*–HI($A^1\Pi_1$) and I–HI($A^1\Pi_1$) complexes.[22]

The H-atom translational energy distribution was computed for the I*–HI($A^1\Pi_1$) excitation energy associated with 266 nm radiation[21] in order to compare with the experimental results.[19] The calculated distribution consisted of two peaks, one corresponding to photolysis on the I*–HI($A^1\Pi_1$) electronic surface and another very small peak shifted to higher kinetic energies by nearly the I*/I spin–orbit splitting, which was the calculated

Effect of Excitation Energy on (HI)$_2$ Dynamics

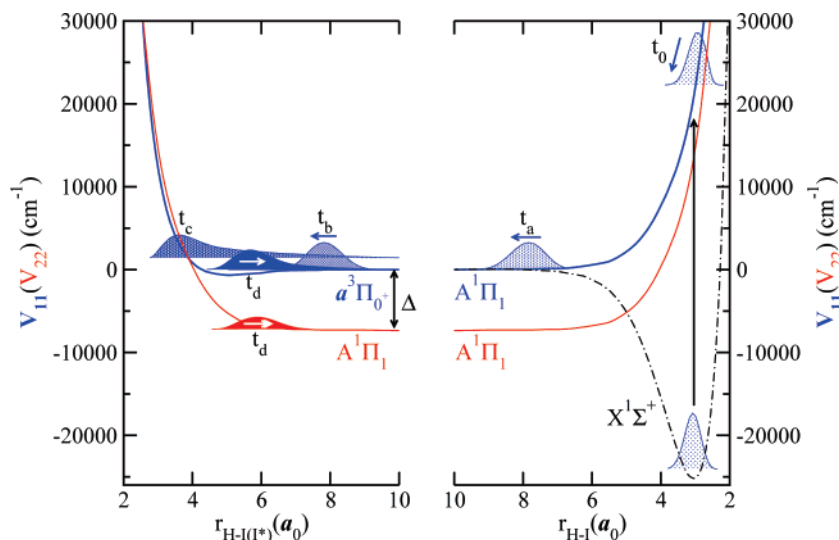*J. Phys. Chem. A, Vol. 112, No. 13, 2008* **2763**

Figure 1. Schematic representation of the I*−HI nonadiabatic photodissociation on the relevant potential energy curves.

analog of the β peak observed experimentally. The calculated β peak accounted for 0.15% of the H-fragment kinetic energy distribution, in good qualitative agreement with the experimental estimate of 0.1−1% for the signal of this peak.[19] The simulations indeed showed that the β peak is produced by nonadiabatic transitions induced by relatively weak intracluster collisions within the I*−HI complex, between the nascent H fragment and I*, which lead to deactivation of I*.[22] A most interesting result of the distribution calculated for excitation with 266 nm radiation was the finding of a high probability of bound I$_2$ product fragments in highly excited rovibrational states. Indeed, about 89% of the photolysis on the I*−HI($A^1\Pi_1$) electronic surface produced bound I$_2$(B) species, while more than half of the nonadiabatic transitions to the I−HI($A^1\Pi_1$) surface led to I$_2$(X) products.[21] It is stressed that highly excited bound Cl$_2$ product fragments were also found in the photodissociation of the Cl−HCl complex.[23]

Interestingly, while the probability of nonadiabatic transitions for excitation with 266 nm wavelength was 0.15%, the average probability of nonadiabatic transitions associated with the whole wave packet (which contains a broad band of energies of a few eV corresponding to the absorption spectrum of the I*−HI-($A^1\Pi_1 \leftarrow X^1\Sigma^+$) electronic transition) was found to be 0.37%.[22] This result suggests a non-uniform behavior of the probability of nonadiabatic transition with the excitation energy of I*−HI. This would not be surprising taking into account the expected dependence of the nonadiabatic process on the conditions in which the H/I* intracluster collisions take place, as pointed out above, and that these collisional conditions will change with the excitation energy.

The aim of the present work is to investigate the possible dependence of the (HI)$_2$ nonadiabatic photodissociation dynamics and its manifestations on the excitation energy of the system. Changing the excitation energy has the effect of changing the conditions in which the H/I* intracluster collisions leading to nonadiabatic transitions take place and, in addition, this parameter has the advantage that it is experimentally tunable by varying the excitation wavelength. To this purpose, we have analyzed the product fragment state distributions of the I*−HI($A^1\Pi_1$) photodissociation in a wide range of excitation energies of the I*−HI($A^1\Pi_1 \leftarrow X^1\Sigma^+$) absorption spectrum. Our goal in this study is twofold. On the one side, to explore how the probability of electronically nonadiabatic transitions, and therefore of I* → I deactivation, is affected by changing the

excitation energy of the parent complex. On the other side, to investigate how the probability of I$_2$ products and their state distributions depend on the excitation energy.

The paper is organized as follows. In Section II the methodology used is described briefly. In Section III, the results are presented and discussed. Some conclusions are drawn in Section IV.

II. Methodology

The wave packet treatment used to simulate the nonadiabatic photodissociation dynamics of I*−HI has been described in detail elsewhere.[22] We shall review it briefly here. Upon excitation of a HI subunit within (HI)$_2$ from the ground HI-($X^1\Sigma^+$)−HI($X^1\Sigma^+$) electronic state to the excited HI($a^3\Pi_{0+}$)−HI($X^1\Sigma^+$) electronic state, photodissociation takes place producing the fragments H + I*−HI($X^1\Sigma^+$).[24] We assume in our model that this first step in the sequential photodissociation of (HI)$_2$ has occurred previously. Our simulation starts by further exciting the I*−HI($X^1\Sigma^+$) complex produced in the above photodissociation step to the I*−HI($A^1\Pi_1$) electronic state, where the HI bond dissociates. The I*−HI($A^1\Pi_1$) electronic surface crosses with the surface of the I−HI($A^1\Pi_1$) complex at the I*−H separation of 3.89 a_0.[8] The two electronic potential surfaces are coupled by the spin−rotation interaction, and they are asymptotically separated by the I*/I spin−orbit splitting Δ = 7341 cm^{-1} (taken from the ab initio configuration interaction calculations of ref 7).

The I*−HI photodissociation process under study is depicted schematically in Figure 1. The I*−HI system is represented in the Jacobi coordinates (r, R, θ), where r is the I*−H bond distance, R is the separation between I and the I*H center of mass, and θ is the angle between the **r** and **R** vectors. These coordinates are shown in Figure 2.

The potential surfaces for the two excited electronic states are modeled as a sum of pairwise interactions.[21] The H−I and H−I* interactions (associated with the $A^1\Pi_1$ and $a^3\Pi_{0+}$ electronic states, respectively) are described by ab initio potential curves,[7] and the I−I and I−I* interactions (corresponding to the $X^1\Sigma_g^+$ and $B^3\Pi_u$ electronic states, respectively) are represented by empirical potentials.[25,26] The wave packet initially prepared in the I*−HI($A^1\Pi_1$) electronic state is propagated on the two coupled electronic surfaces, assuming zero total angular momentum for the system.
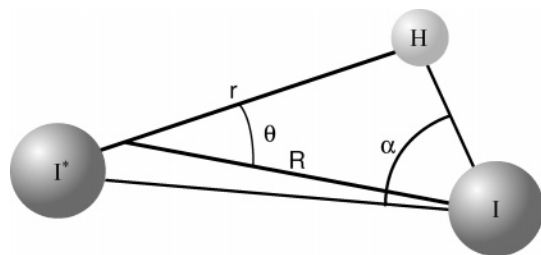
Figure 2. Schematic picture of the (r, R, θ) Jacobi coordinates used to represent the I*−HI system. The angle α between the I−H and I−I* axes indicates the initial orientations of the H atom.

The spin−rotation coupling between the two electronic surfaces is represented by the expression[21]

$$V_{12} = \left\langle {}^3\prod\nolimits_{0+} | \hat{H}_{SR} | {}^1\prod\nolimits_1 \right\rangle =$$

$$\delta(r) \left\langle {}^3\prod\nolimits_{0+} | \hat{H}_{SR} | {}^3\prod\nolimits_1 \right\rangle = -\frac{\hbar^2 \delta(r)}{\sqrt{2}\,\mu_{HI} r^2} [J(J+1)]^{1/2} \quad (1)$$

where $\hat{H}_{SR}$ is the spin−rotation operator, μ_{HI} is the reduced mass associated with r, and J is the collisional angular momentum quantum number associated with the H/I* collision. It is noted that with the Jacobi coordinates (r, R, θ) used (Figure 2) the angular momentum associated with the angle θ coincides with the collisional angular momentum J. Because of spin−orbit coupling, the $|^1\Pi_1\rangle$ state of HI has some character of the $|^3\Pi_1\rangle$ state, and the admixture of this character depends on the HI bond length r. The $\delta(r)$ function describes such a dependence, and it was calculated through ab initio multireference internally contracted configuration interaction calculations including spin−orbit coupling (MRCI-SO). A detailed discussion of the $\delta(r)$ function and its calculation was given in ref 22.

The wave packet is represented on a rectangular grid of 540 × 100 equally spaced points in the r and R coordinates, respectively, in the ranges $1.47a_0 \le r \le 45.12a_0$ and $8.86a_0 \le R \le 12.61a_0$. For the angular coordinate, a representation on a grid of 320 points corresponding to a Gauss−Legendre quadrature in the range $0° \le \theta \le 180°$ was chosen. This angular discrete variable representation, combined with a finite basis representation consisting of 210 Legendre polynomials, was used to calculate the action of the angular momentum operator onto the wave packets. The wave packet propagation was carried out using the Chebychev polynomial expansion method, up to a final time $t_f = 70$ fs with a time step $\Delta t = 2$ fs.[27]

After propagating the wave packet until it reaches the asymptotic region, it is projected out onto all possible product fragment states at the I*−HI excitation energies of interest. For each excitation energy, such degenerate states correspond to the product fragments H + I + I* and H + I*−I [i.e., I_2(B^3\Pi_u)] in the upper excited electronic surface, associated with I*−HI, and to the product fragments H + I + I and H + I−I [i.e., I_2(X^1\Sigma_g^+)] in the electronic surface populated after a nonadiabatic transition takes place (the one associated with I−HI). Details on the wave packet projection procedure have been given elsewhere.[21,27−29] In this way, the state distributions of the product fragments on the two electronic surfaces are obtained for a specific excitation energy.

We should mention that because of the large number of product states involved the wave packet projection is a computationally expensive task and its extension to several energies can become prohibitive. For this reason, we have rewritten our projection codes to run on computers with massively parallel processors. We have used the message passing interface (MPI)
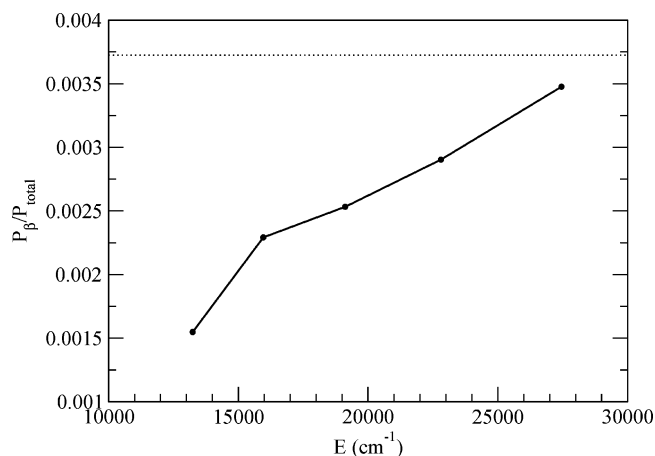

Figure 3. Relative probability of nonadiabatic transitions vs the excitation energy E of I*−HI. The horizontal dotted line corresponds to the everage relative probability (0.37%) obtained for the whole wave packet, which contains all of the excitation energies of the absorption spectrum. See the text for details.

library[30] to subdivide the projection domain into partial blocks, performing the independent operations of each block, and then combining the corresponding results. A speed-up with respect to the serial processor time of a factor of 30 was achieved. A full discussion on the implementation and the performance of the codes is given elsewhere.[31]

In ref 21, the fragment state distributions produced with the 266 nm radiation wavelength used experimentally were reported.[19] The I*−HI excitation energy reached with that wavelength was $E = 13\,244$ cm^{-1} ($E = 0$ corresponds to H + I* + I separated atoms). In the present work, we have computed fragment state distributions for four higher excitation energies, namely, 15 962, 19 117, 22 808, and 27 450 cm^{-1}, which correspond to I*−HI excitation with 248, 230, 212, and 193 nm radiation wavelengths, respectively. This range of excitation energies covers a wide region of the I*−HI($A^1\Pi_1 \leftarrow X^1\Sigma^+$) absorption spectrum, which extends from ~10 000 to ~45 000 cm^{-1}.[22]

III. Results and Discussion

A. Variation of the Probability of Nonadiabatic Transitions. For a given excitation energy E, the probability of electronically nonadiabatic transition (or equivalently, of I* → I deactivation) is obtained as the sum of the probabilities of photodissociation into all possible degenerate states (at energy E) of the fragments H + I + I and H + I_2(X). Such a probability, P_β, corresponds to the area of the calculated β peak. Dividing this probability by the total probability of photodissociation on the two coupled electronic surfaces (which is equivalent within a constant factor to the total photodissociation cross section), one obtains the relative probability of nonadiabatic transition, P_β/P_{total}. This quantity provides the fraction of probability of nonadiabatic transitions out of the whole photodissociation process, and it is suitable in order to analyze how the intensity of the nonadiabatic process depends on the excitation energy. The P_β/P_{total} relative probability versus E is shown in Figure 3 for five different excitation energies, namely, the four energies studied here plus the excitation energy reported in ref 21.

The curve of Figure 3 shows that the relative probability of nonadiabatic transition increases monotonically with E, from 0.15% for $E = 13\,244$ cm^{-1} to 0.35% for $E = 27\,450$ cm^{-1}. This result comes to confirm the previous hypothesis that the behavior of the nonadiabatic transition probability with E is not

uniform.[21,22] The horizontal dotted line in Figure 3 indicates the average value (0.37%) of the relative probability obtained from the whole wave packet, which contains all of the excitation energies of the absorption spectrum. Because the average probability is 0.37%, it is expected that the relative probability will still increase further above this average for energies $E > 27\,450$ cm^{-1}.

The intensity of the β peak observed experimentally for excitation with 266 nm wavelength was very low (with relative probability of 0.1−1% of the total signal of the H-atom translational energy spectrum). The experimental implication of the result of Figure 3 is that the intensity of the nonadiabatic process, and therefore of its signature, the β peak, can be enhanced remarkably by exciting the system to higher energies.

The increase of the relative probability of nonadiabatic transitions with E can be understood by resorting to elementary concepts of collision theory.[32,33] For the H/I* intracluster collision that induces the electronically nonadiabatic transition, the collisional angular momentum J can be expressed as

$$J = \mu_{\mathrm{HI}} v b \tag{2}$$

where v is the collision velocity and b is the collision impact parameter. Excitation of the I*−HI complex takes place through an $A^1\Pi_1 \leftarrow X^1\Sigma^+$ electronic transition of the HI chromophore, which means that essentially all of the excitation energy is placed in the H−I bond. Because of the H/I mass ratio, the dissociating H fragment carries most of the excitation energy initially deposited in the H−I bond as kinetic energy, namely, $\epsilon_k^{\mathrm{H}} = [m_{\mathrm{I}}/(m_{\mathrm{H}} + m_{\mathrm{I}})]E$. Thus, the excitation energy directly determines the velocity v of the H/I* collision because, assuming that I* does not move appreciably before the H/I* collision, we have $v = (2\epsilon_k^{\mathrm{H}}/\mu_{\mathrm{HI}})^{1/2} = (2E/m_{\mathrm{H}})^{1/2}$. When the excitation energy E increases, v increases correspondingly, and following eq 2 it causes a linear increase of J. Because the intensity of the spin−rotation coupling depends directly on J (see eq 1), the increase of J with the excitation energy has the effect of increasing the intensity of the coupling and therefore of enhancing the probability of nonadiabatic transitions.

B. Variation of the Probability of I₂ Products. The behavior with E of the probability of the different photodissociation pathways, namely, dissociation into H + I₂(B) and H + I + I* fragments on the upper excited electronic surface, and dissociation into H + I₂(X) and H + I + I fragments on the lower electronic surface, has been analyzed. As above, in the analysis we have used the relative probability $P_{\mathrm{pathway}}/P_{\mathrm{total}}$. The corresponding probabilities versus E are shown in Figure 4.

In the case of I₂ product fragments, Figure 4 displays three probability curves corresponding to I₂ formation in bound, quasibound, and in bound plus quasibound rovibrational states. It is found that practically all of the I₂(B) and I₂(X) photofragments are produced in bound rovibrational states, over the range of energies E studied. Therefore, most of the I₂(B) and I₂(X) final products are stable species.

The behavior of the probability of I₂(B) products displays a slow decrease with E. The decrease of the I₂ probability is an expected result. Indeed, as the energy available for the fragments increases with E, survival of I₂ products is expected to decrease because of the increase of the energy transferred to the I₂ bond both by the recoil of the H fragment and by the H/I* collisions. Interestingly, however, the decrease of the I₂(B) relative probability with E is rather slow, going from 89% for $E = 13244$ cm^{-1} to about 60% for $E = 27450$ cm^{-1}. Thus, the probability of I₂(B) photoproducts remains remarkably high over a wide range of excitation energies. The implication of this finding is
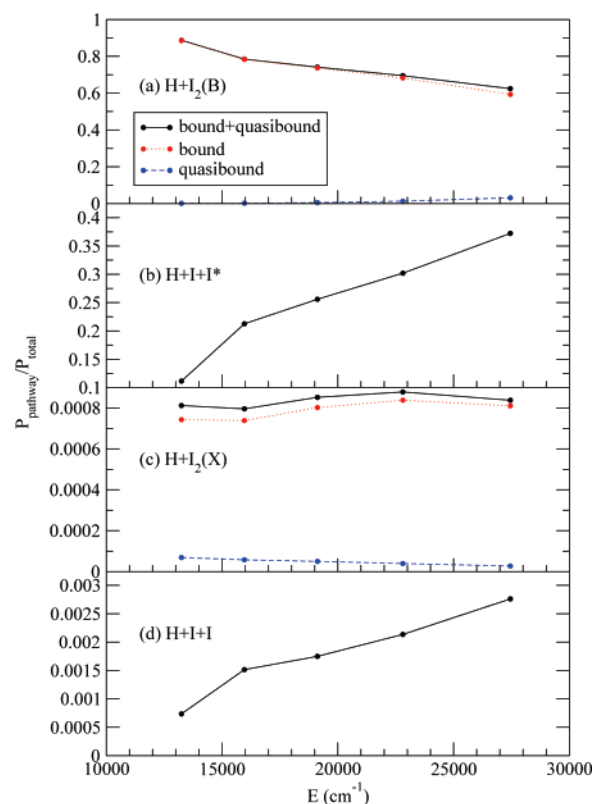

Figure 4. Relative probabilities vs E for the photodissociation pathways leading to (a) H + I₂(B) products, (b) H + I + I* products, (c) H + I₂(X) products, and (d) H + I + I products. In panels a and c, the three curves show the probability of I₂ product fragments in bound rovibrational states (dotted line), quasibound rovibrational states (dashed line), and the sum of probabilities in bound and quasibound rovibrational states (solid line).

that experimental detection of stable, bound I₂(B) species as products of the photodissociation would still be possible with a high probability as the excitation energy is increased.

The I*−I equilibrium distance within the I*−HI($X^1\Sigma^+$) complex is rather large, ∼5.1 Å, and it is associated with vibration in the region of very highly excited bound rovibrational states of the spectrum of the I₂(B) potential. Thus, when excitation occurs through the I*−HI($A^1\Pi_1 \leftarrow X^1\Sigma^+$) electronic transition, a distribution of these highly excited rovibrational states is initially prepared for the I*−I bond. With this highly excited initial preparation, one could intuitively expect a rather fast decrease of the survival probability of I₂(B) products with increasing excitation energy, in contrast to the results shown in Figure 4. A more detailed analysis of the photodissociation dynamics mechanisms reveals, however, a more favorable situation for the survival of I₂(B) fragments as E increases.

Analysis of the wave packet dynamics showed that dissociation of H within I*−HI is dominantly a direct process, or at most involving rather weak H/I* collisions.[22] In these conditions, the energy imparted to the I*−I bond after the photodissociation process is essentially the share of the recoil energy due to the H−I dissociation within I*−HI. Such a share of the recoil energy in the I*−HI center-of-mass is $E_{\mathrm{recoil}} = [m_{\mathrm{H}}/(m_{\mathrm{H}} + 2m_{\mathrm{I}})]E \sim (1/255)E$. For the excitation energies $E = 15\,962$, $19\,117$, $22\,808$, and $27\,450$ cm^{-1}, the corresponding recoil energies become $E_{\mathrm{recoil}} = 63$, 75, 89, and 108 cm^{-1}, respectively. We note that, in addition, roughly half of these recoil energies will become translational energy of the I₂(B) fragment center of mass, so the remaining energy available for I₂(B) rovibrational excitation is still rather low even at high excitation energies.
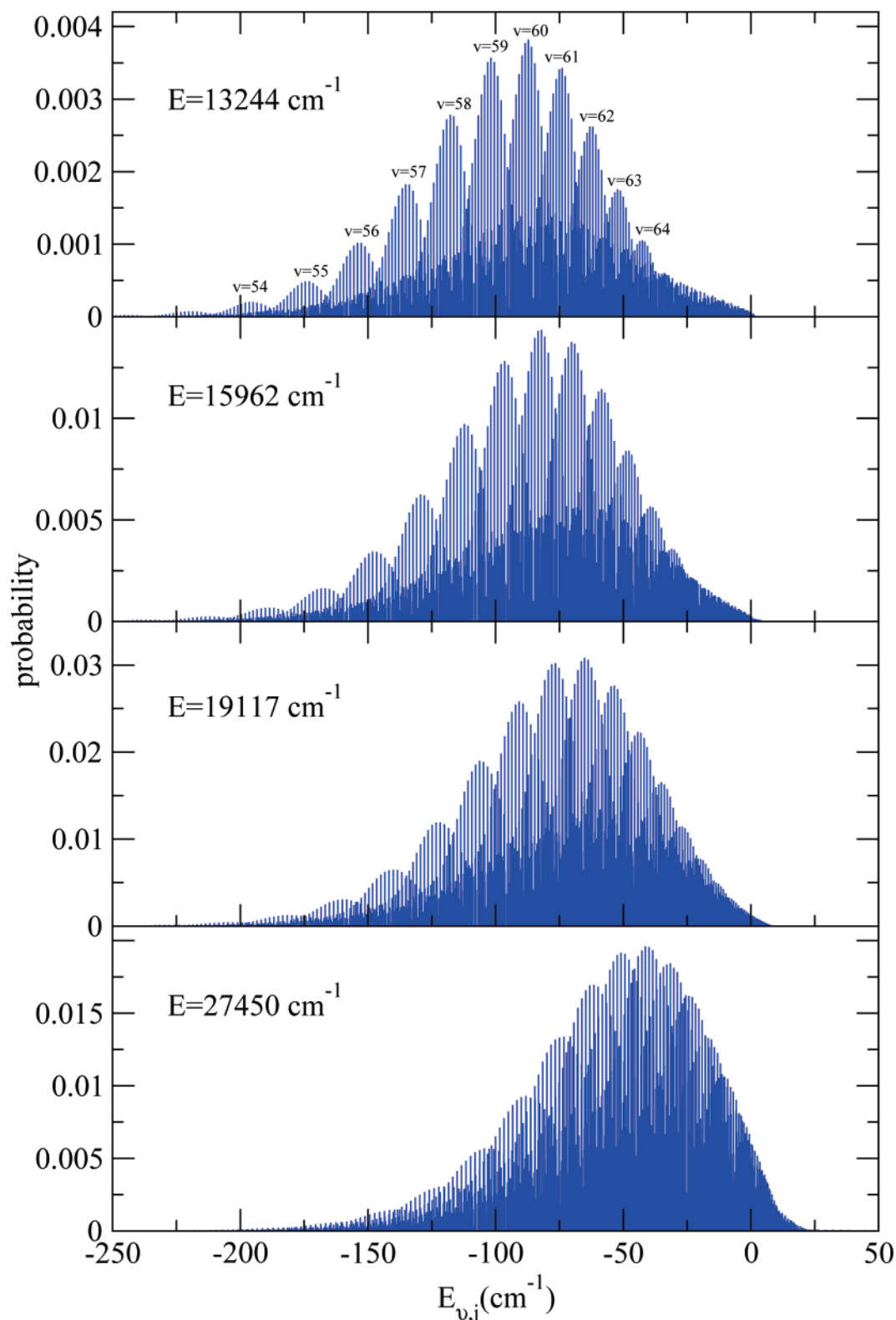
Figure 5. Rovibrational state distributions of the $I_2(B)$ product fragment for four excitation energies E of I^*-HI. Negative and positive $E_{v,j}$ energies correspond to bound and quasibound rovibrational states of $I_2(B)$, respectively. $E_{v,j} = 0$ corresponds to the $I_2(B)$ dissociation limit. The most intense vibrational bands have been assigned and labeled by their corresponding vibrational quantum number.

Thus, the small amount of energy available for the $I_2(B)$ fragment because of the direct photodissociation mechanism explains the slow decrease of the survival probability of $I_2(B)$ products with increasing E. In this sense, for low E $I_2(B)$ would be produced with a final distribution of highly excited rovibrational states similar to the one initially prepared, and this final

state distribution would get gradually hotter as E increases, leading to a slow damping of the $I_2(B)$ survival probability.

The relative probability of $I_2(X)$ fragments produced upon nonadiabatic transitions remains rather constant around 0.08% with increasing E (see Figure 4c). In addition to the relative probability $P_{I_2(X)}/P_{total}$ shown in Figure 4c, one can also analyze

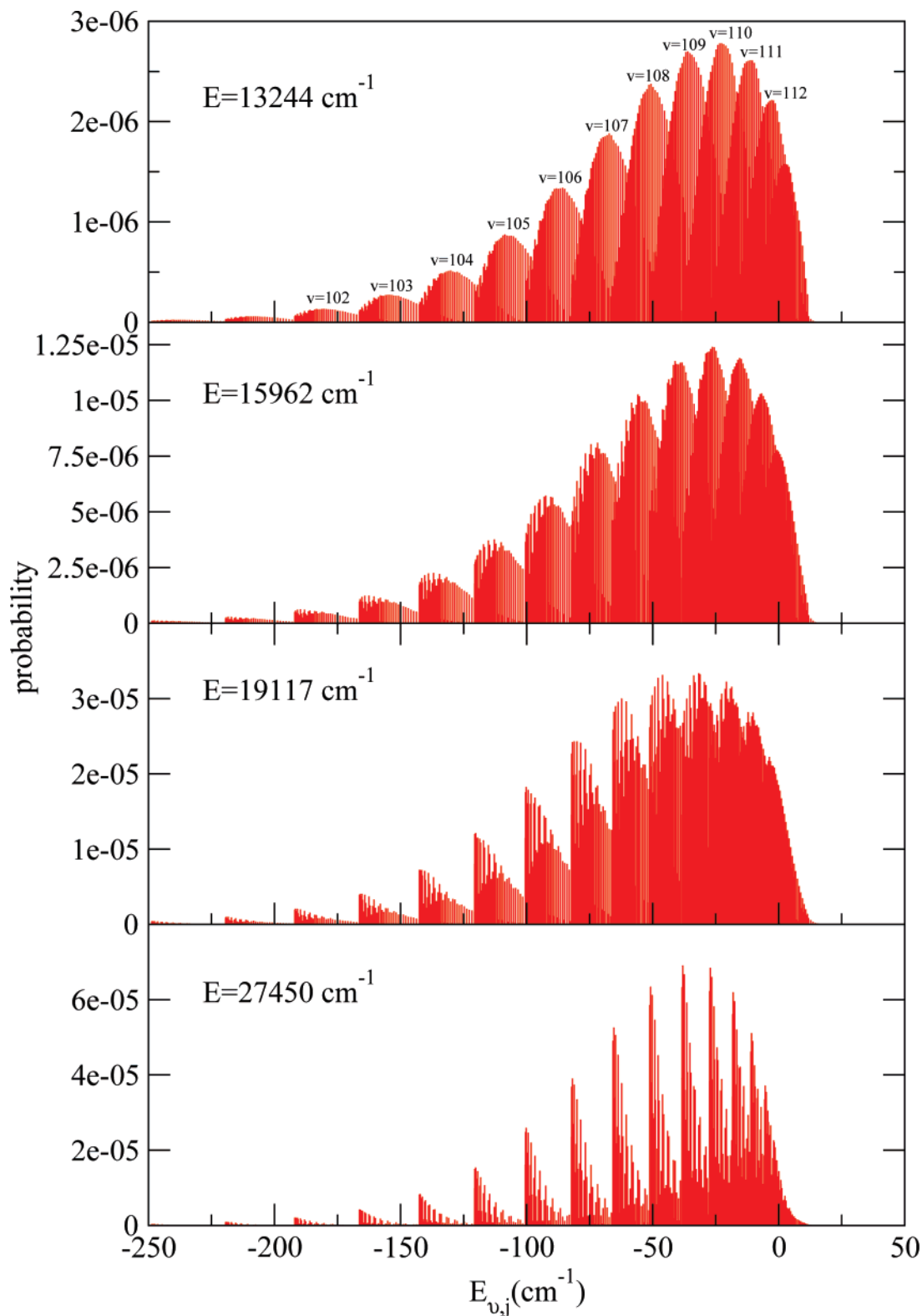Effect of Excitation Energy on (HI)$_2$ Dynamics

J. Phys. Chem. A, Vol. 112, No. 13, 2008 **2767**

Figure 6. Same as Figure 5 for the I$_2$(X) product fragment. $E_{v,j} = 0$ corresponds to the I$_2$(X) dissociation limit.

the behavior with E of the fraction of I$_2$(X) products out of the probability of nonadiabatic transitions, $P_{I_2(X)}/P_\beta = (P_{I_2(X)}/P_{total})/(P_\beta/P_{total})$, obtained by dividing the relative probabilities of Figures 4c and 3. The analysis of $P_{I_2(X)}/P_\beta$ provides information about the fraction of I$_2$(X) products within the signal of the β peak associated with nonadiabatic transitions as the excitation energy increases. The results of Figures 3 and 4c show that $P_{I_2(X)}/P_\beta$ decreases as E increases, as does the fraction of I$_2$(B) fragments of Figure 4a discussed above. Indeed, a fraction of

~50% ($P_{I_2(X)}/P_\beta = 0.08\%/0.15\%$) leads to I$_2$(X) products for E = 13244 cm^{-1}, while this fraction drops to ~25% (0.08%/ 0.35%) for $E = 27450$ cm^{-1}. The fractions of I$_2$(X) products in the β peak are lower than those of I$_2$(B) fragments in Figure 4a for the same E, and the damping of the I$_2$(X) fraction with increasing E is also faster. The reason is that the nonadiabatic transition is mediated by a H/I* intracluster collision, which causes some more energy transfer to the I$-$I bond, in addition to the recoil energy. However, still a relatively large fraction

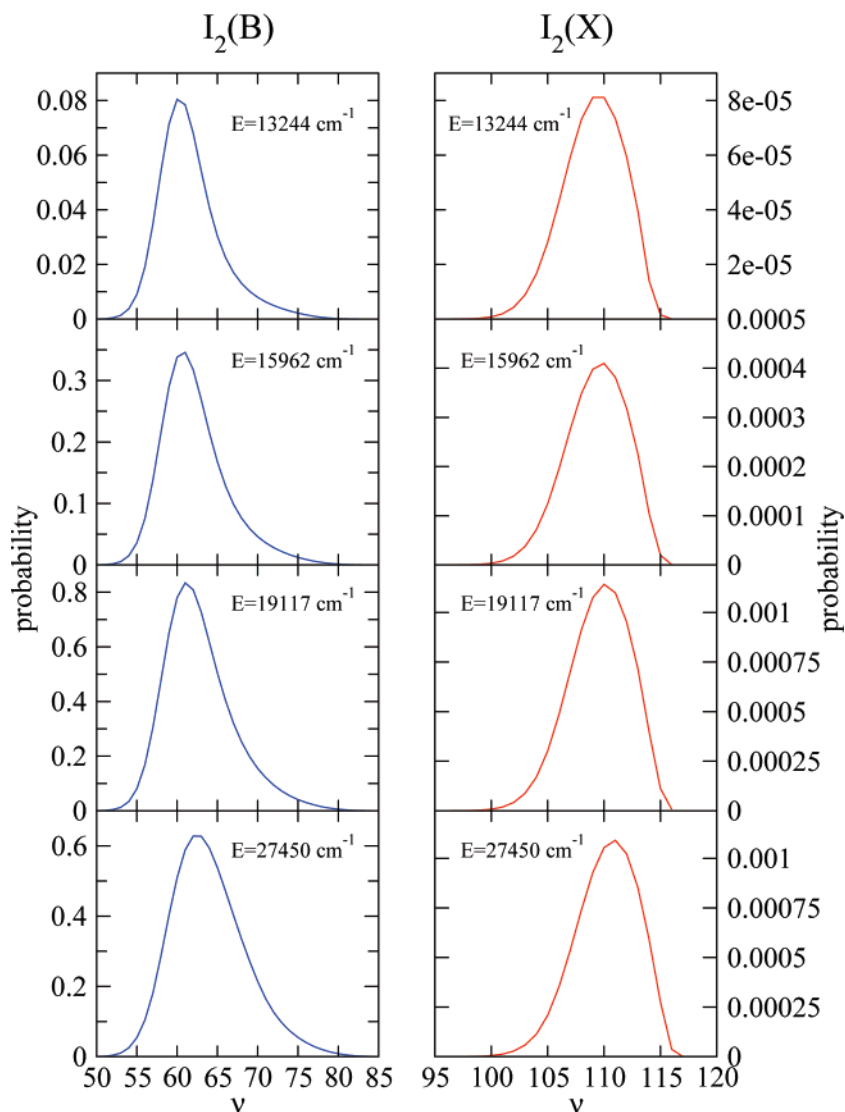$I_2(B)$ $I_2(X)$

Figure 7. Vibrational distributions associated with the $I_2(B)$ fragment (left panels) and with the $I_2(X)$ fragment (right panels) for four excitation energies of I*−HI.

of $I_2(X)$ products (∼25%) is found in the β peak for high excitation energies. This is consistent with the previous finding[22] that most of the H/I* collisions leading to nonadiabatic transitions are relatively weak, so the additional energy transfer to the nascent $I_2(X)$ fragment is not high.

The relative probability of photodissociation into H + I* + I and H + I + I fragments increases monotonically with E (Figure 4b and c). This behavior is directly related to the decrease of the survival probability of I_2 fragments with increasing E. Indeed, those photodissociation events where the I_2 fragment does not survive as E becomes higher contribute to the increase of the probability of dissociation into three atomic fragments.

C. Product Fragment State Distributions. In the following, we shall analyze the behavior of the state distributions of the different products with the excitation energy. Figures 5 and 6 show the rovibrational state distributions of the $I_2(B)$ and $I_2(X)$ products, respectively, for four excitation energies along the range studied.

The distributions of Figures 5 and 6 are composed of a series of vibrational bands, each of them consisting of a rotational progression. As anticipated above, the distributions populate the energetically highest bound rovibrational states of $I_2(B)$ and I_2-

(X), as well as the energetically lowest quasibound rovibrational states. The effect of increasing E on the $I_2(B)$ distributions is a gradual, rather slow increase of the rovibrational excitation of the $I_2(B)$ products, as pointed out before. This increase of the rovibrational excitation is mainly an increase of rotational excitation, as we shall see below, and causes the maximum of the $I_2(B)$ distributions to shift from $E_{v,j} = -85$ cm^{-1} for $E = 13244$ cm^{-1} to $E_{v,j} = -40$ cm^{-1} for $E = 27450$ cm^{-1}. However, the overall excitation and the position of the maximum of the $I_2(X)$ distributions change rather little as E increases. As a result, while the $I_2(X)$ distribution is substantially more excited than the $I_2(B)$ one for $E = 13244$ cm^{-1}, both the $I_2(B)$ and $I_2(X)$ distributions populate a similar energy range and have their maxima at nearly the same energy position for $E = 27450$ cm^{-1}.

It is interesting to note that while the shape of the $I_2(B)$ distributions does not change much with E, this variation is remarkably more pronounced in the case of the $I_2(X)$ distributions. The variations in the $I_2(X)$ distributions are caused mainly by a rotational cooling effect. Interference effects that occur in the photodissociation pathways leading to both $I_2(B)$ and $I_2(X)$, but having a greater influence in the $I_2(X)$ products, also contribute to the variations of the $I_2(X)$ distributions, although
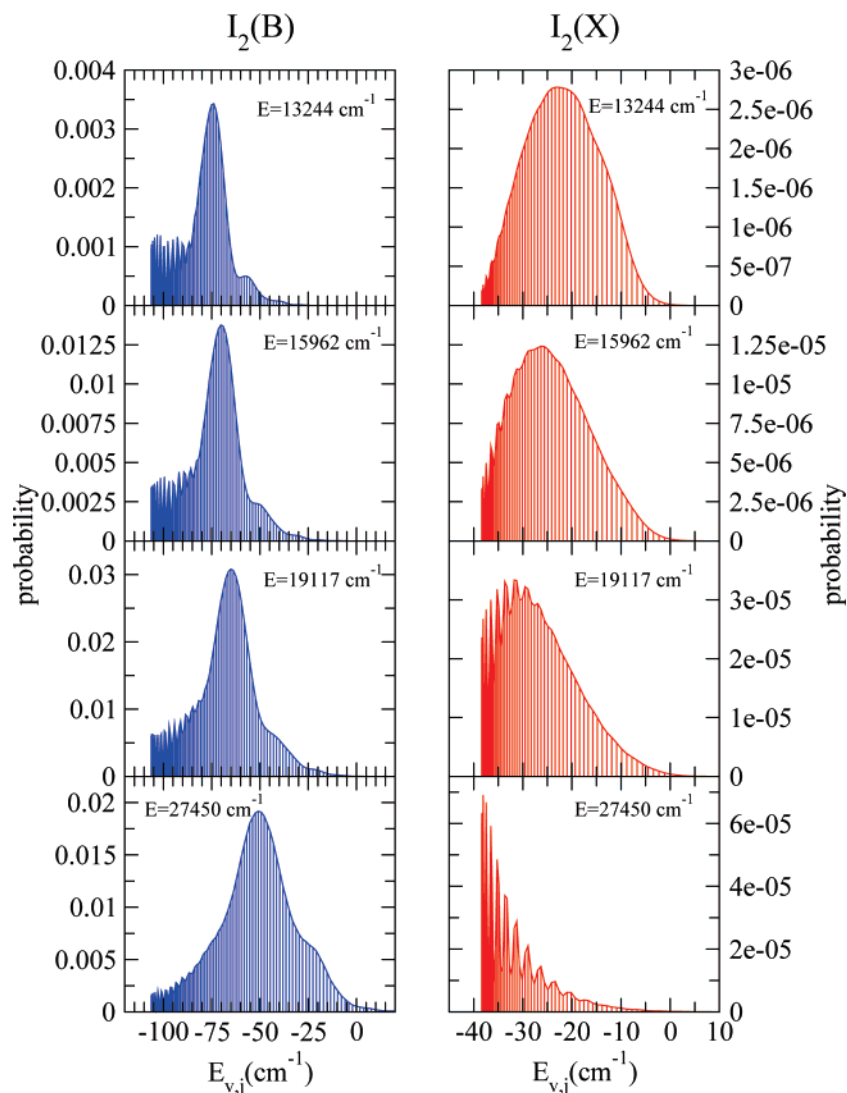
Figure 8. Rotational progressions associated with the $v = 61$ vibrational band of the $I_2(B)$ rovibrational distribution (left panels) and with the $v = 110$ vibrational band of the $I_2(X)$ rovibrational distribution (right panels) for four excitation energies. The rotational progressions show envelope of each stick rotational progression has also been plotted.

to a lesser extent. Both the rotational cooling and the interference effects will be discussed in detail below.

Vibrational distributions can be extracted from the rovibrational distributions of Figures 5 and 6 by summing over the j states, and they are shown in Figure 7. These distributions show the range of vibrational levels populated in the $I_2(B)$ and $I_2(X)$ fragments. These ranges are $v = 50-80$ in the case of $I_2(B)$ and $v = 100-116$ in the case of $I_2(X)$. The maxima of the I_2-(B) and $I_2(X)$ distributions occur around $v = 61$ and $v = 110$, respectively, the $I_2(X)$ product being far more excited vibrationally. The shape of the vibrational distributions of both products hardly changes with increasing E. Only a slight excitation is found, which shifts the maxima of the $I_2(B)$ and $I_2(X)$ distributions from $v = 61$ to $v = 62$ and from $v = 110$ to $v = 111$, respectively.

The distributions of Figures 5 and 6 are congested spectra, which make a detailed analysis of the rotational distributions difficult. Thus, in order to analyze the behavior of the rotational populations, we have examined separately the different vibrational bands of each rovibrational distribution of Figures 5 and 6. We found that the rotational progressions associated with all of the vibrational bands of a given rovibrational distribution present a similar behavior and shape. As typical examples, we have extracted from the distributions of Figures 5 and 6 the

rotational progressions associated with the most populated vibrational bands, $v = 61$ for $I_2(B)$ and $v = 110$ for $I_2(X)$, and they are displayed in Figure 8. The rotational progressions show two interesting features. One feature is that both the $I_2(B)$ and $I_2(X)$ progressions display a pattern of oscillations in the region of low and medium rotational states, which becomes more pronounced as E increases in the $I_2(X)$ progressions. The other feature is that while the $I_2(B)$ progressions become rotationally hotter with increasing E, on the contrary, the $I_2(X)$ progressions get rotationally colder as E increases. Although the gradual rotational cooling can be appreciated in the $I_2(X)$ rovibrational distributions of Figure 6, the pattern of oscillations in the region of low rotational states is less clear in the $I_2(X)$ rovibrational distributions or even hidden in the $I_2(B)$ distributions of Figure 5.

In order to discuss the above effects in more detail, it is more convenient to deal with rotational distributions in the domain of the j quantum number rather than in the domain of the $E_{v,j}$ energy of Figure 8. Because the rotational behavior of all of the vibrational bands within each rovibrational distribution is similar, a convenient choice is to deal with rotational distributions obtained from the rovibrational ones by averaging over the vibrational states. The averaged rotational distributions are
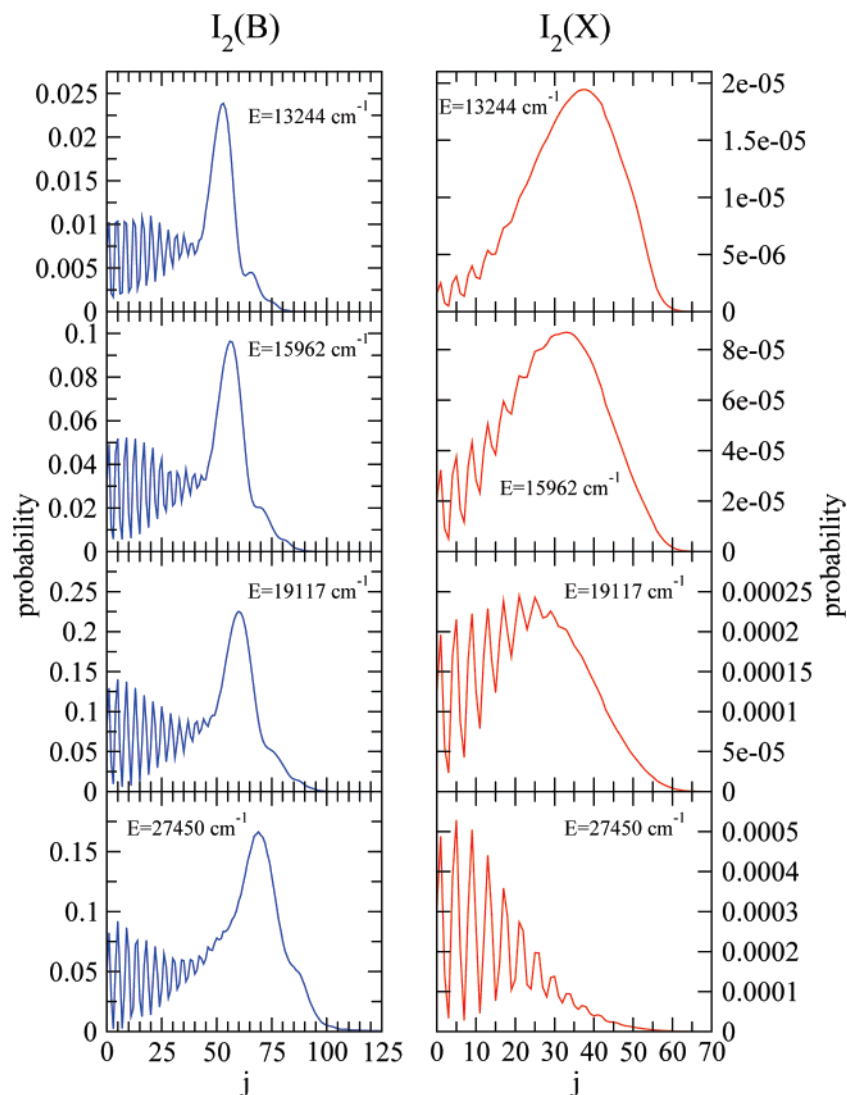
Figure 9. Averaged rotational distributions associated with the $I_2(B)$ fragment (left panels) and with the $I_2(X)$ fragment (right panels) for four excitation energies of I*−HI.

shown in Figure 9. As expected, these distributions are very similar in shape to the rotational progressions of Figure 8.

The averaged rotational distributions of the $I_2(B)$ and $I_2(X)$ fragments show qualitatively larger differences than the vibrational ones. The $I_2(B)$ product is rotationally more excited than $I_2(X)$, and the distributions of $I_2(B)$ populate a range of j states remarkably larger than those of $I_2(X)$. This different behavior is related to the specific fragmentation mechanisms leading to the $I_2(B)$ and $I_2(X)$ products. The $I_2(B)$ fragments are produced mainly through direct dissociation of the H atom at angles α of the H−I bond (see Figure 2) sufficiently large for which the H fragment is able to overcome the I* obstacle. From these large initial orientations α, the recoiling H fragment produces a relatively intense torque on the $I_2(B)$ product. This mechanism gives a rise in $I_2(B)$ to a rotational excitation that is higher than the vibrational one. On the contrary, the $I_2(X)$ fragment is produced after a nonadiabatic transition induced by a H/I* intracluster collision, which implies smaller initial angles α of H−I, leading to a significantly less-intense torque on $I_2(X)$. This mechanism produces higher vibrational excitation than the rotational one on the $I_2(X)$ product, as found in Figures 7 and 9.

The averaged rotational distributions of $I_2(B)$ change rather little in shape with E, similar to the $I_2(B)$ vibrational distributions, just becoming gradually hotter as E increases because of

an increase of the intensity of the torque produced by the recoiling H on $I_2(B)$. The small changes of the $I_2(B)$ vibrational and rotational populations with E reflect the slow variation of the rovibrational distributions of Figure 5. The variation of the $I_2(X)$ rotational population with E is much more significant, and it is the origin of the more pronounced variation of the rovibrational distributions of Figure 6 (provided that the $I_2(X)$ vibrational distributions change little with E as well). Actually, it is the rotational cooling effect already mentioned that is responsible for the variations in the $I_2(X)$ distributions.

As in the case of the rotational progressions of Figure 8, the averaged rotational distributions of both $I_2(B)$ and $I_2(X)$ display a pattern of oscillations in the population of low and medium j states. Such a pattern vanishes gradually for high j states. This pattern would be originated by interference between low rotational states of I_2, which are excited by torques of low or medium intensity produced by the H dissociation on the I_2 fragment. The interference would be induced by weak H/I* collisions (unable to break the I_2 fragment) and would occur between components of the wave packet associated with different initial orientations of the H−I bond axis, but leading to the same final rotational state.

It is interesting that the interference pattern survives in all of the distributions of Figure 9, after averaging the corresponding rovibrational distributions over ∼27 vibrational states for $I_2(B)$
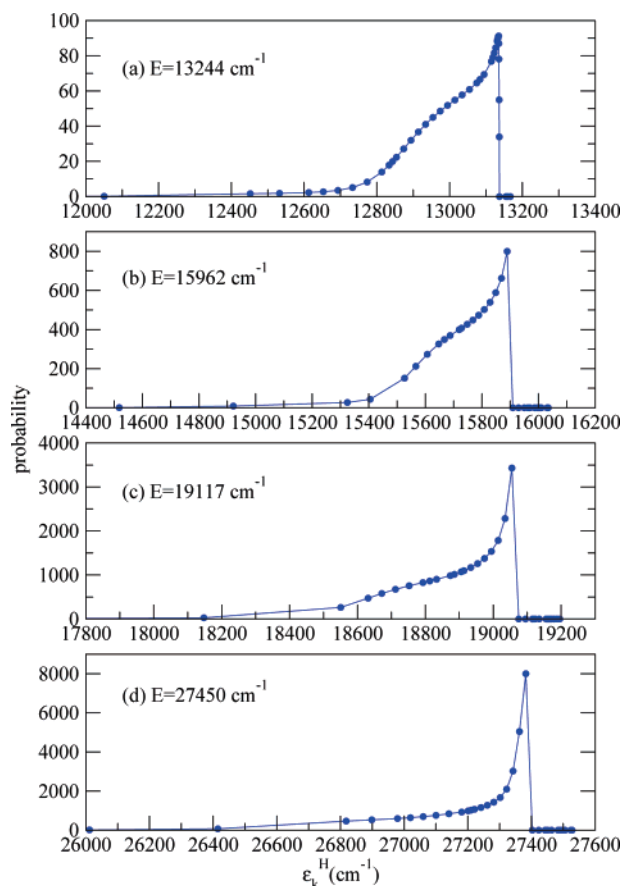
Effect of Excitation Energy on (HI)$_2$ Dynamics

J. Phys. Chem. A, Vol. 112, No. 13, 2008 **2771**

Figure 10. H-atom translational energy distributions produced by photodissociation of I*−HI into H + I + I* fragments for four excitation energies of I*−HI.
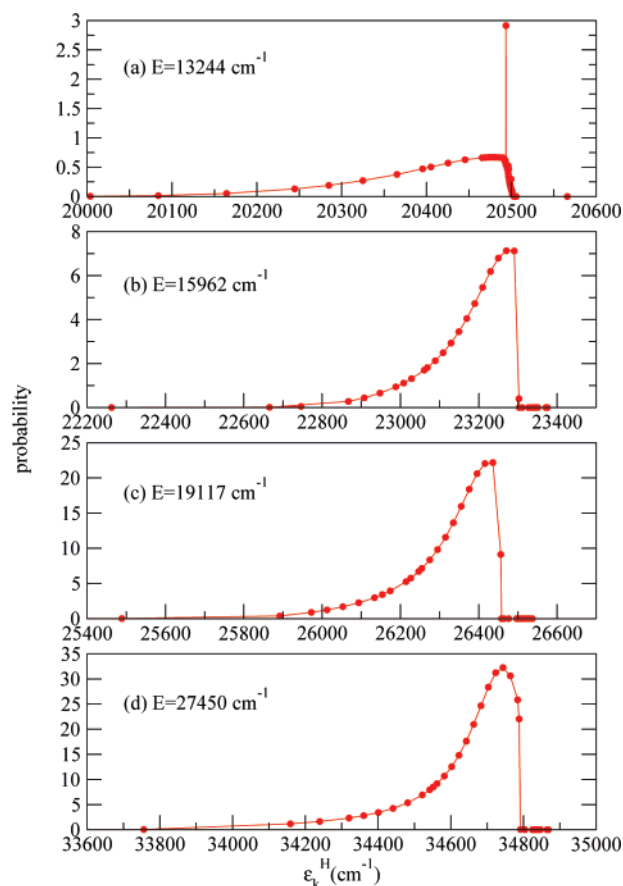

Figure 11. H-atom translational energy distributions produced by photodissociation of I*−HI into H + I + I fragments for four excitation energies of I*−HI.

and ∼15 vibrational states for I$_2$(X). This indicates that the same interference pattern, with coincident positions of the oscillations, occurs in all of the vibrational bands of the rovibrational distributions. The positions of the oscillations in the patterns of the I$_2$(B) and I$_2$(X) distributions are also coincident, reflecting that the origin of the interference pattern is the same in both cases, namely, a weak H/I* intracluster collision. The effect of increasing E does not affect the position of the oscillations at low j states, only causing the appearance of new oscillations at higher j. It is stressed that similar rotational interference patterns have been found in the rotational distributions of Kr−Br and Ar−I radical fragments produced upon photodissociation of Kr−HBr[34] and Ar−HI[35] clusters.

As the H fragment dissociation becomes more and more direct (when the initial orientation α of H−I increases) and the intensity of the H/I* collision decreases or even disappears, the intensity of the torque on I$_2$ increases and higher rotational states are excited. However, those high rotational states no longer interfere themselves significantly because of the absence of the H/I* collision, and the pattern of oscillations vanishes in the I$_2$ distributions for high j. When E increases, the weak H/I* collisions inducing interference become more intense, and the effect of the interference pattern gradually reaches higher rotational states in the distributions of both I$_2$(B) and I$_2$(X). Interestingly, however, while the population of high (noninterfering) rotational states remains in the I$_2$(B) distributions when E increases, it vanishes in the I$_2$(X) distributions, causing their rotational cooling.

The gradual quenching of the population of high rotational states in the I$_2$(X) distributions with increasing E might be due to the following mechanism. In the very beginning of the

photodissociation process (during the first 10 fs, before the H/I* collision), the recoiling H fragment would excite a range of rotational states in the nascent I$_2$(B) fragment because of the torque produced on I$_2$(B). The range of rotational states excited depends on the intensity of the torque, which is determined by the initial orientation of the H−I bond, as pointed out before. Because there is a distribution of initial H−I orientations, it is expected that both low and high rotational states will be excited in the nascent I$_2$(B) fragment, as corroborated by the averaged I$_2$(B) rotational distributions of Figure 9, produced mainly by direct dissociation. When the H atom reaches the region of interaction with I*, a H/I* collision occurs leading to a nonadiabatic transition that deactivates I* within I$_2$(B), producing an I$_2$(X) fragment. This collision and the subsequent nonadiabatic transition might induce transfer of rotational excitation from the highest rotational states populated in the nascent I$_2$(B) to vibrational excitation of the final I$_2$(X) product (which might also involve breaking of the I$_2$(X) fragment). By increasing E, the intensity of the H/I* collision increases correspondingly, which would make the energy transfer from rotational to vibrational (and even continuum) states in I$_2$(X) more effective. The above mechanism would explain the quenching of population in the highest rotational states and therefore the gradual rotational cooling found in the I$_2$(X) distributions with increasing E.

The H-atom kinetic energy distributions produced upon photodissociation of I*−HI into H + I* + I and H + I + I fragments are shown in Figures 10 and 11, respectively. For each excitation energy, the maxima of the distributions of Figure 11 are separated from the maxima of the distributions of Figure 10 by an amount of energy nearly equal to the spin−orbit

2772 *J. Phys. Chem. A, Vol. 112, No. 13, 2008*

López-López et al.

splitting Δ. This result reflects the fact that the H fragment acquires nearly all of the I* excitation when it is deactivated to I through the electronically nonadiabatic transition.

The effect of increasing E on the distributions is that their maxima appear at kinetic energies gradually lower with respect to the corresponding excitation energy E. This result indicates that the H fragment transfers more energy to the atomic iodine fragments (both as recoil energy of the I fragment produced from H–I dissociation and through the H/I* collision) as E increases. In addition, the tail of the distributions toward lower kinetic energies increases in intensity and extent, indicating that the H fragment is cooled down more effectively with increasing E. These tails are likely to be originated by multiple collisions (at least two, and probably more) between the H fragment and the iodine atoms because the H/I mass ratio makes it unlikely to transfer in a single collision as much energy as that shown by the distribution tails. In particular, the shoulder appearing at kinetic energies between 200 and 300 cm^{-1} to the left of the main peak of the distributions of Figure 10 is probably originated by a superposition of probability associated with a first H/I* collision and probability associated with a second weak collision of the H fragment recoiling backward with I.

IV. Conclusions

The effect of the excitation energy on the nonadiabatic photodissociation of (HI)$_2$ has been investigated. For this purpose, the nonadiabatic photodissociation dynamics of the I*–HI complex left behind after dissociation of the first HI moiety within (HI)$_2$ has been simulated by means of wave packet calculations. Probabilities and product fragment state distributions of the different photodissociation pathways were computed for several excitation energies of I*–HI over a wide range of the absorption spectrum. The aim was to explore how the change of the photodissociation conditions (by varying the complex excitation energy) affects the final outcome of the nonadiabatic process.

The simulations show that the probability of electronically nonadiabatic transitions increases substantially with the excitation energy (by a factor larger than 2) over the range studied. This result is explained in terms of the specific nature of the spin–rotation coupling responsible for the nonadiabatic transitions, whose intensity is enhanced with increasing excitation energy. It is also found that the probability of bound I$_2$ fragments as products of the photodissociation decreases slowly with increasing excitation energy, and it remains remarkably high over the range of energies analyzed. The I$_2$ fragments are produced dominantly in highly excited bound rovibrational states. The I$_2$ product state distributions manifest interference effects between rotational states. In addition, a rotational cooling effect is found in the I$_2$ fragment distributions produced after nonadiabatic transitions. The intensity of both the rotational cooling and the interference effects is found to increase with the excitation energy, causing substantial variations in the I$_2$ state distributions produced upon nonadiabatic transitions. Finally, the findings reported here should be observable and could aid future experimental investigations on the nonadiabatic dynamics in this type of cluster.

References and Notes

(1) Domcke, W.; Yarkony, D. R.; Hoppel, H. *Conical Intersections: Electronic Structure, Dynamics and Spectroscopy* (Adavanced Series in Physical Chemistry); World Scientific Publishing Co.: Singapore, 2004.

(2) Balasubramanian, K.; Han, M.; Liao, M. Z. *J. Chem. Phys.* **1987**, *86*, 4979.

(3) Baugh, D.; Koplitz, B.; Xu, Z.; Wittig, C. *J. Chem. Phys.* **1988**, *88*, 879.

(4) Sumathi, K.; Balasubramanian, K. *J. Chem. Phys.* **1990**, *93*, 1837.

(5) Dyall, K. G.; Taylor, P. R.; Faegri, K.; Partridge, H. *J. Chem. Phys.* **1991**, *95*, 2583.

(6) Meuwly, M.; Hutson, J. M. *Phys. Chem. Chem. Phys.* **2000**, *2*, 441.

(7) Alekseyev, A. B.; Liebermann, H.-P.; Kokh, D. B.; Buenker, R. J. *J. Chem. Phys.* **2000**, *113*, 6174.

(8) Balakrishnan, N.; Alekseyev, A. B.; Buenker, R. J. *Chem. Phys. Lett.* **2001**, *341*, 594.

(9) Klos, J. A.; Chalasinski, G.; Szcześniak, M. M.; Werner, H.-J. *J. Chem. Phys.* **2001**, *115*, 3085.

(10) Underwood, J.; Chastaing, D.; Lee, S.; Boothe, P.; Flood, T. C.; Wittig, C. *Chem. Phys. Lett.* **2002**, *362*, 483.

(11) Zeimen, W. B.; Klos, J.; Groenenboom, G. C.; van der Avoid, A. *J. Phys. Chem. A* **2003**, *107*, 5110.

(12) Zeimen, W. B.; Klos, J.; Groenenboom, G. C.; van der Avoid, A. *J. Chem. Phys.* **2003**, *118*, 7340.

(13) Alekseyev, A. B.; Liebermann, H.-P.; Wittig, C. *J. Chem. Phys.* **2004**, *121*, 9389.

(14) Underwood, J.; Chastaing, D.; Lee, S.; Wittig, C. *J. Chem. Phys.* **2005**, *123*, 084312.

(15) Alekseyev, A. B.; Kokh, D. B.; Buenker, R. J. *J. Phys. Chem. A* **2005**, *109*, 3094.

(16) de Nalda, R.; Izquierdo, J. G.; Durá, J.; Bañares, L. *J. Chem. Phys.* **2007**, *126*, 021101.

(17) Alekseyev, A. B.; Liebermann, H.-P.; Buenker, R. J.; Yurchenko, S. N. *J. Chem. Phys.* **2007**, *126*, 234102.

(18) Alekseyev, A. B.; Liebermann, H.-P.; Buenker, R. J. *J. Chem. Phys.* **2007**, *126*, 234103.

(19) Chastaing, D.; Underwood, J.; Wittig, C. *J. Chem. Phys.* **2003**, *119*, 928.

(20) Moore, C. E. *Atomic Energy Levels*; National Bureau of Standards: Washington, D.C., 1971.

(21) López-López, S.; Prosmiti, R.; García-Vela, A. *J. Chem. Phys.* **2007**, *126*, 161102.

(22) López-López, S.; Prosmiti, R.; García-Vela, A. *J. Chem. Phys.* **2007**, *127*, 184307.

(23) Jungwirth, P.; Ždánská, P.; Schmidt, B. *J. Phys. Chem. A* **1998**, *102*, 7241.

(24) Actually, excitation of HI($X^1\Sigma^+$) within (HI)$_2$ occurs via a perpendicular transition that populates both the $A^1\Pi_1$ and $a^3\Pi_{0+}$ excited states of HI. Excitation to the $A^1\Pi_1$ state produces H + I–HI($X^1\Sigma^+$) fragments, while excitation to the $a^3\Pi_{0+}$ state gives rise to H + I*–HI-($X^1\Sigma^+$) fragments. In our simulations, we do not consider the channel producing I–HI($X^1\Sigma^+$) fragments because further photodissociation of this complex does not involve the nonadiabatic dynamics that we are interested in.

(25) *NIST Standard Reference Database Number 69*, June 2005 Release, http://webbook.nist.gov/chemistry/.

(26) Gruebele, M.; Zewail, A. H. *J. Chem. Phys.* **1993**, *98*, 883.

(27) Juanes-Marcos, J. C.; García-Vela, A. *J. Chem. Phys.* **2000**, *112*, 4983.

(28) Juanes-Marcos, J. C.; García-Vela, A. *J. Chem. Phys.* **2001**, *115*, 5692.

(29) Juanes-Marcos, J. C.; García-Vela, A. *J. Phys. Chem. A* **2002**, *106*, 5445.

(30) *MPICH2, An Implementation of the Message-Passage Interface (MPI)*, (http://www-unix.mcs.anl.gov/mpi/mpich/).

(31) López-López, S. *Fotodisociacion UV de agregados de vdW con enlaces de hidrogeno*. Ph.D. Thesis, Universidad Complutense de Madrid, 2007.

(32) Child, M.S. *Molecular Collision Theory*; Academic Press: London, 1974.

(33) Goldstein, H. *Classical Mechanics*; Adison-Wesley Press: Reading, MA, 1951.

(34) López-López, S.; García-Vela, A. *J. Chem. Phys.* **2004**, *120*, 660.

(35) López-López, S.; Prosmiti, R.; García-Vela, A. *J. Chem. Phys.* **2004**, *121*, 1802.